Report on MCMP 2015 proposal:

What can remote sensing tell us about water, nitrogen and phosphorous in corn: a comparison of platforms and algorithms to help corn growers

Dr. Bruno Basso
Dept. Geological Sciences and W.K. Kellogg Biological Station
Michigan State University

1.0 Rationale

Precision agriculture (PA) is the application of geospatial techniques and sensors (e.g., geographic information systems, remote sensing, GPS) to identify variations in the field and to deal with them using site-specific strategies. In particular, high-resolution satellite imagery is now more commonly used to study these variations for crop and soil conditions. However, the availability and the often-prohibitive costs of such imagery would suggest an alternative product for this particular application in PA. Specifically, images taken by low altitude remote sensing platforms such as planes, or small unmanned aerial systems (UAS), are shown to be a potential alternative given their low cost of operation in environmental monitoring, high spatial and temporal resolution, and their high flexibility in image acquisition programming.

2.0 Objectives

The objective of this study was to evaluate the capability of remote sensing from different platform (UAV, planes and satellite) in capturing spatial variability of corn growth. A variety of algorithms based on vegetation indices were compared. A new cluster procedure was developed to identify areas on which the crop model can be executed.

3.0 Methodology

3.1 Field site description and experimental layout

Studies were completed in cooperation with two farmers for this investigation: one near Portland, Michigan and the other near St. John's, Michigan.

Portland, Michigan

The first experiment described in this report was completed during the 2015 growing season in a 68 acre field near Portland, Michigan. Conover loam covers the majority of the central and northernmost sections of this field with 0 to 2 % slopes (52% of the field) and 2-6% slopes

(10%). This soil is characterized by up to 12" of loam underlain by clay loam, is considered somewhat poorly drained and depth to the water table is 12 to 24". Other areas of this field are similar to the Conover loam in texture and depth to a confining layer although the Celina loam (35%), located in the southern and central portions of the field, is considered well-drained. The Brookston loam, located in the southwestern portion of the field near a pond, is very poorly drained and covers approximately 2% of the field.

St. John's, Michigan

A second experiment was completed on a 13 acre portion of a larger corn field near St. John's, Michigan. The soil at this location is comprised almost entirely (93%) of Metamora-Capac sandy loam which is characterized by 0-4% slopes and is underlain by a clay loam at 9". This soil is characterized as somewhat poorly drained, has high available water storage, but is not prone to ponding. Small portions of the study area are classified as Oakville fine sands (5%) with 0-6% slopes and as Capac loam (1.6%).

The three Nitrogen application rates in this experiment were 22 gal/acre, 0 gal/acre and 22 gal/acre + side dress application (22 gal/acre) later in the growing season. Each of these application rates was replicated three times in the same field. The entire study area also received applications of Amonium Thiosal sulfer (2 gal/acre) and 10-34-0-2N-sulfur (12 gal/acre). Pioneer variety 9807 corn was planted May 2, 2015 at a seeding rate of 32,700 seeds/acre.

3.2 Field observations

Sample collection

Corn biomass samples were collected five times during the 2015 growing season in 13 locations in the Portland field to "ground truth" areas of interest identified in airborne photos. Samples were also collected five times at 9 locations in the St. John's field to sample each of the treatment replicates. At each field the cumulative location of each plant along a 1.5m length of a row was noted and the entire aboveground biomass of each plant along the measured length was collected. Samples were then dried, ground and analyzed for total Nitrogen. GPS coordinates of each sample location were noted so that samples could be taken on subsequent dates in the same location. Corn cobs were separated from stover for the fourth sampling for Nitrogen analysis and kernels were separately counted and analyzed for Nitrogen for the fifth sample date.

Yield map

A map was created with data collected from the yield monitor mounted on the farmer's combine at the end of the growing season. Yield data collected with this combine is located at points 0.8m along rows and from rows that are spaced 12m apart. A kriging algorithm was then used to interpolate values between these data points to create a yield map. This yield map was used to evaluate vegetation indices to determine to what degree they reflected the final yield. Imagery

collected on different dates was also compared with the yield map in the same manner to determine the stage of crop growth most closely related to the final yield.

3.3 Remote sensing

Drone imagery

Unmanned aerial vehicles (UAV) were used to collect imagery in these corn fields with a variety of sensors including LiDAR, RGB and multi-spectral cameras. The multi spectral camera was used to take images at the same time that plant samples were collected, in order to compare data from two locations on a finite time system. A smaller UAV was used to employ the RGB camera. These images were primarily used to observe variation in the field throughout the growing season. We employed LiDAR to evaluate crop height at different times over the course of the growing season, however technical difficulties arose with this technology. This process exhibited limited success, but needs improvement. Throughout the season, mechanical and technological failure led to significant problems in data collection. As systems become more advanced our expectation is that more complete data sets will be collected.

Other remote sensing imagery and analysis

Airborne photos representing the RGB (red/green/blue) wavelengths were obtained from Airscout for ten dates during the growing season. The original photo and the original red, green and blue wavelengths were used along with eleven additional vegetation indices that were developed from the original photo by calculating different wavelength combinations (as shown in Table 1). Data from these processed images for each of the 10 days were then compared to the final yield map to determine the index and the date that were most closely associated with the final yield.

Table 1. Vegetation Indices

Vegetation Index	**Wavelength combinations**
r	R* / (R* + G* + B*)
g	G* / (R* + G* + B*)
b	B* / (R* + G* + B*)
RVI	(Red / Green)
AVRI	Red / (Blue * Green) * 100
VNDVI	(Green - Red) / (Green + Red)
R_G	Red - Green
G_B-R_G	(Green - Blue) / (Red - Green)
G_B	Green - Blue
2G-R-Blue	2Green - Red - Blue
Hue	Cos^{-1}(2R-G-B/(2*Sqrt([R^2 + G^2 + B^2 - R*G - G*B-R*B]))

R*= R/Rmax, G* = G / Gmax, B* = B / Bmax

Nitrogen Uptake Map

Nitrogen uptake maps were created with the analytical results of samples that were collected five times through the growing season according to the following equation:

(Biomass kg/m^2) (%N)= N uptake

N uptake maps were used to evaluate those areas of the field where plants were utilizing the most nitrogen, whether areas of high and low N uptake were stable and whether those areas were consistent with the final yield map. Figure 1 shows a N uptake map developed with samples collected July 1. The size of sample location markers shown in Figure 1 relates to the magnitude of N uptake at that location on that date and not to the size of the area compared with airborne imagery.

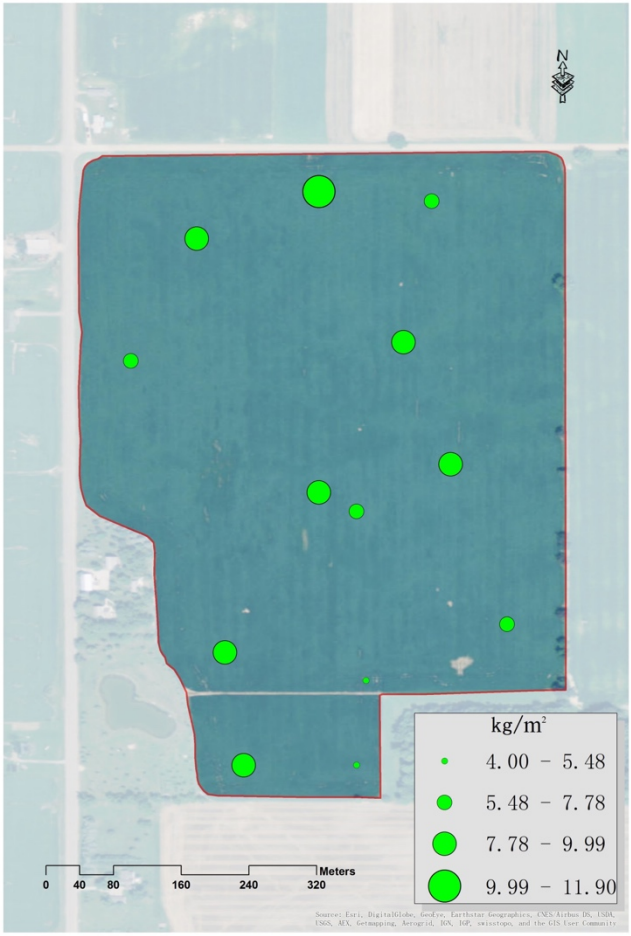

Figure 1. Nitrogen uptake (July 1)

4.0 Results and Discussion

Yield Map

Data obtained from the yield monitor was used to create the yield map shown in Figure 2. The mean yield value was 221 bu/ac, it ranged from 38 to 284 bu/ac and exhibited a standard deviation of 20 bu/ac. This dataset was used to evaluate the degree to which the calculated vegetation indices reflected the final yield. Indices calculated on different dates were also compared to this yield map in the same manner. The individual classes into which pixels in the image are divided each represent 25% of the overall total.

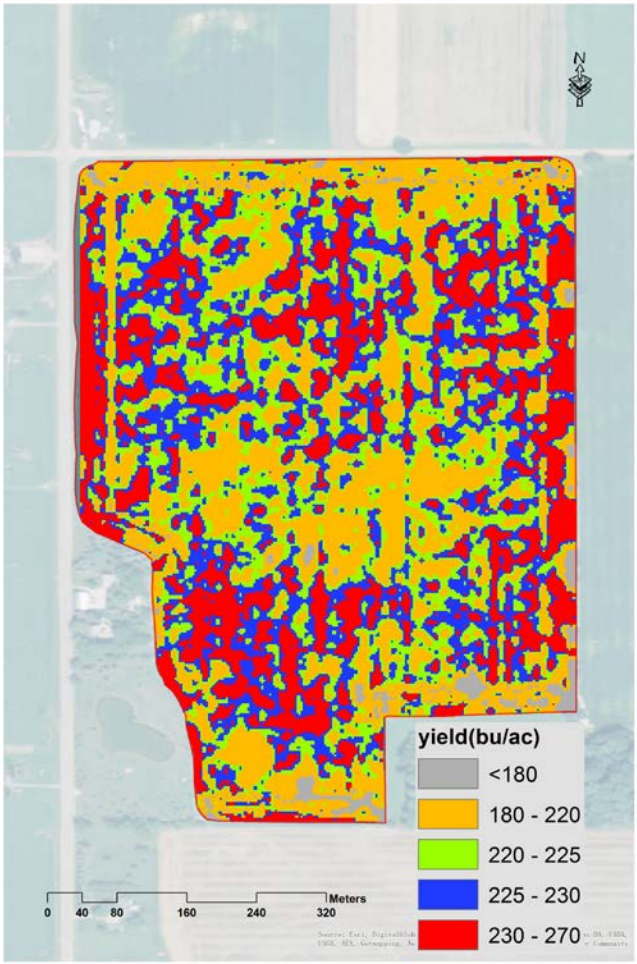

Figure 2. Corn yield map

Final yield sample results

Table 2 shows mean values for biomass, kernel count and %N obtained at final harvest for the thirteen areas sampled.

Table 2. Mean values at final harvest

	Grain			Whole plant
Sample	%N	Mass (g)	Kernel count	Mass (g)
1	1.31	142.9	423	257.4
2	1.24	151.1	489	167.2
3	1.36	147.4	461	277.6
4	1.28	153.7	465	252.3
5	1.28	139.0	451	251.7
6	1.31	117.8	400	209.1
7	1.28	152.5	480	272.4
8	1.28	127.2	434	233.6
9	1.37	159.3	462	289.6
10	1.23	152.5	454	265.5
11	1.21	134.3	450	237.3
12	1.29	148.6	459	259.8
13	1.24	160.8	489	280.4

The location of areas within the field with the most robust plant growth generally remained constant throughout the growing season when compared to other areas of this field. Samples collected at sites 1 and 9 were consistently the highest and samples collected at sites 2, 6, and 8 were consistently the lowest over the length of the growing season. However site 13 was consistently lower than the rest of the field until the final samples were collected, at which time it had the highest biomass and kernel count but remained among the lowest sites for % N. This is thought to be due to the fact that destructive sampling involves moving farther from the initial sample location with each subsequent sample.

Relationship between remote sensing and field data

Samples collected in the field were compared with Airscout photos taken on the date as near as possible to the sample collection date. The difference between the date of sampling and the Airscout photo collection ranged from as little as zero (collected the same day) up to a difference of 10 days. Data collected in the field represents single points and was converted to a $4m^2$ area for this analysis. Problems in precisely matching GPS coordinates of both the photo and the field data resulted in a loss of precision with this method. However, analysis of data collected June 17 showed a correlation coefficient of 0.25 which represents a positive relationship between these two datasets.

Vegetation Indices and yield

Correlation coefficients were calculated to compare fourteen visual Airscout image vegetation indices with the corn yield data. This analysis was completed for photos collected on 10 dates throughout the growing season and October 8 was identified as the date most closely related to the final yield as illustrated in Figure 3. Negative correlation coefficients are considered as having the same meaning as positive ones and are represented in this figure with positive values. The largest coefficient value (r=0.44) was obtained on October 8 for the VNDVI index which was identified as the index best able to represent corn growth. VNDVI was calculated as:

VNDVI = (Green-Red) / (Green+Red)

Figure 3. Correlation between vegetation indices and corn yield

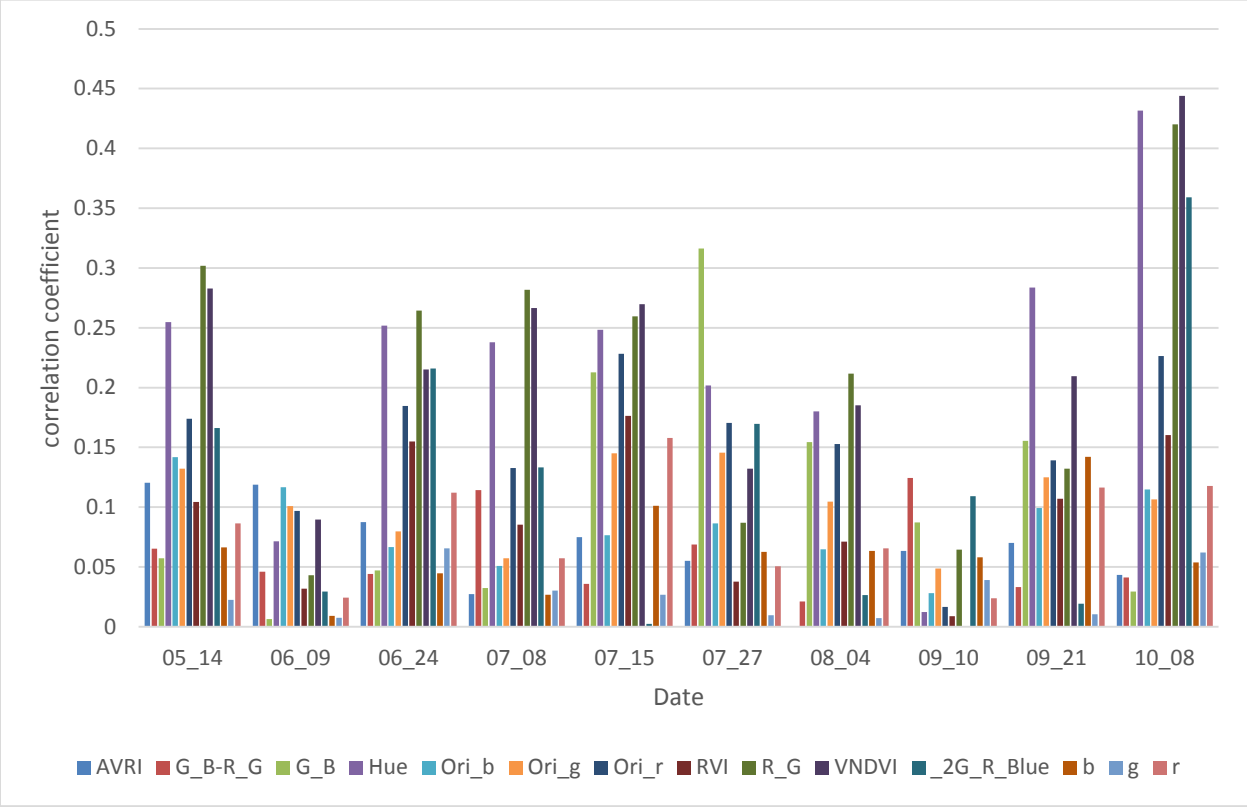

Nitrogen Uptake and Yield

We calculated the correlation coefficient between nitrogen uptake of samples collected on five different dates with final corn yield as shown in the following figures. Data from field samples

was converted to areas representing 4m^2 for comparison with yield data. The best fit was obtained for samples collected July 1 (r^2=0.42) as shown in Figure 4.

Figure 4. Correlation between Nitrogen uptake (July 1) and final yield

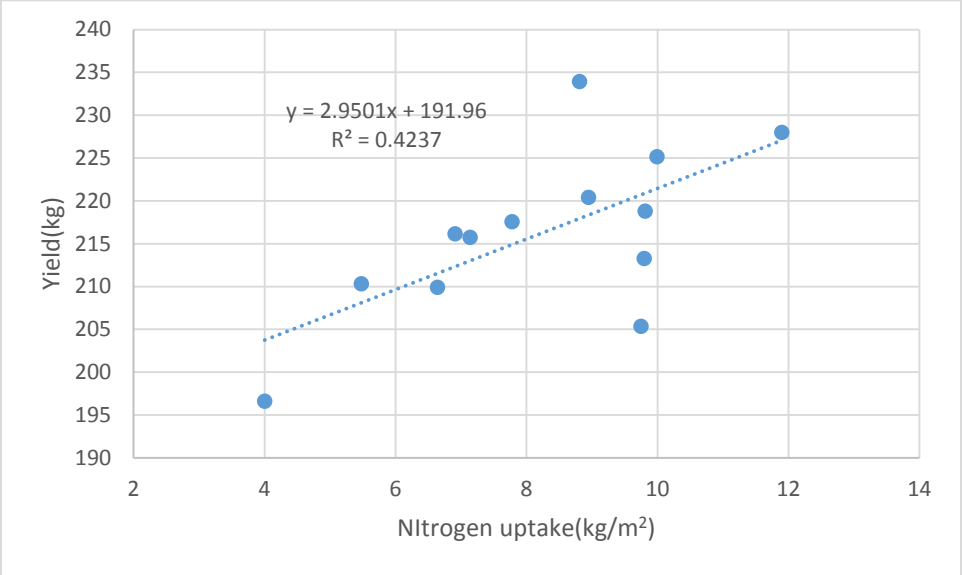

Nitrogen uptake and vegetation indices

We analyzed the relationship of nitrogen uptake to original red reflectance or VNDVI at the dates closest to the field sample date. Here we show red reflectance as an example of this analysis. The nitrogen uptake and red reflectance at individual dates have a low, but not significant relationship. The combination of nitrogen uptake for field samples collected June 17 and red reflectance for imagery collected June 24 had the best relationship among these scenarios (r^2=0.55) as shown in Figure 5.

Figure 5. Nitrogen uptake (June 17) and original red reflectance (June 24)

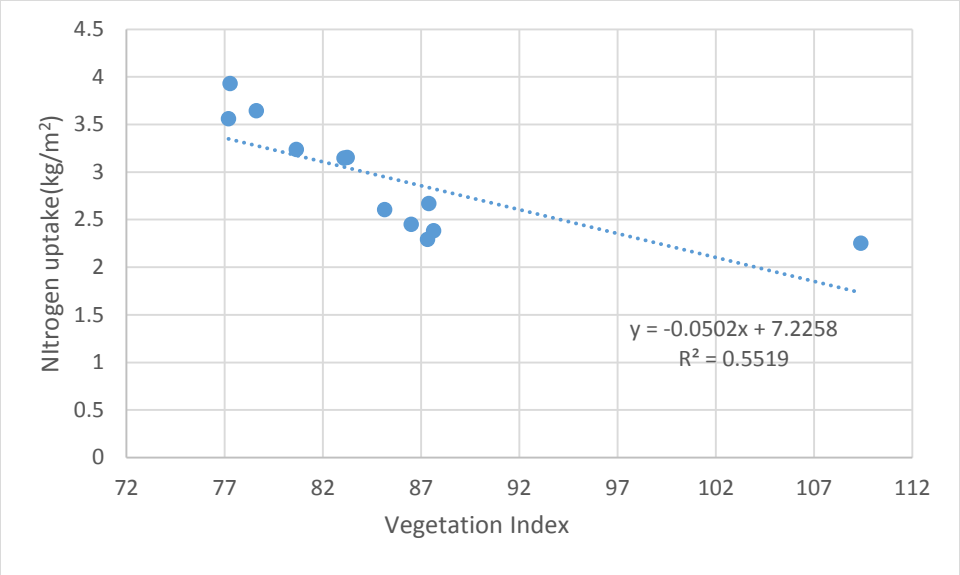

The comparison between the image collected with RapidEye satellite and the one collected with Airscout is presented in Fig 6.

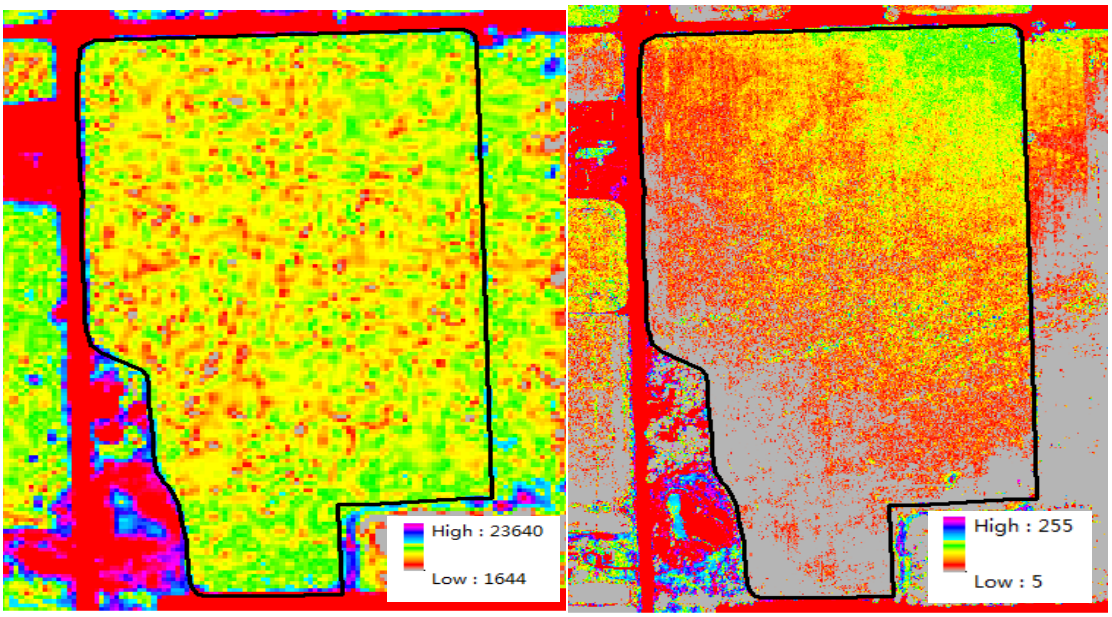

Figure 6. Satellite image compared with airborne image.

Crop modeling

The SALUS model was used to simulate the corn grain yield of the field. Model input data on soil and weather were obtained from USDA-SURGGO data and from the Mesonet weather station. Agronomic management data was obtained from the farmer. The measured and simulated data from the different fields data are presented in fig. 7. The SALUS model was able to closely predict the yield within the season (in September) and at the harvest time.

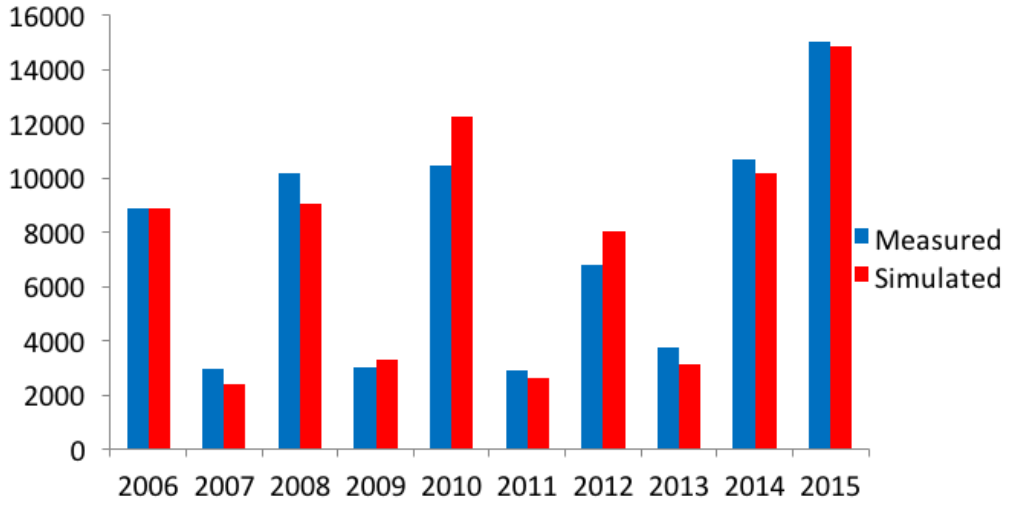

Figure 7. Measured and simulated yield data using the SALUS model.

St. John's, Michigan

Final harvest data is summarized in the following table for the three fertilizer treatments. Treatments 1 and 2 were not significantly different for any of the parameters measured and treatment 3 was significantly different from both treatments 1 and 2 for all measurements.

Table 3. Mean values for final harvest-St. John's

	Grain			Whole plant
	%N	Mass (g)	Kernel count	Mass (g)
Treatment 1 (22 gal/acre + side dress)	1.16	144.6	533	246.7
Treatment 2 (22 gal/acre)	1.11	138.2	516	238.8
Treatment 3 (0 gal/acre)	0.87	81.6	387	148.2

5.0 Conclusions and Recommendations

The study described a comprehensive study carried out at the field scale to assess the role of remote sensing in capturing yield variation across space and time. The vegetation indices provided a limited role in predicting yield, while the SALUS crop model was able to closely predict the corn and soybean yields in two different fields. The image from satellite was significantly less informative compared to the airborne image due to coarser spatial resolutions. The limited selection of satellite image dates due to cloud cover confirmed the inability of such a system to provide timely information. The drone imagery was valuable but the complexity and the problems related to the image capture and image post processing treatments makes this stem still challenging. We plan to continue this investigation with the goal of linking remote sensing with crop model to understand and manage the spatial and temporal variability of crop yield.

6.0 Appendices

Nitrogen Uptake and Yield

Figure A1. Correlation between N uptake (June 17) and yield

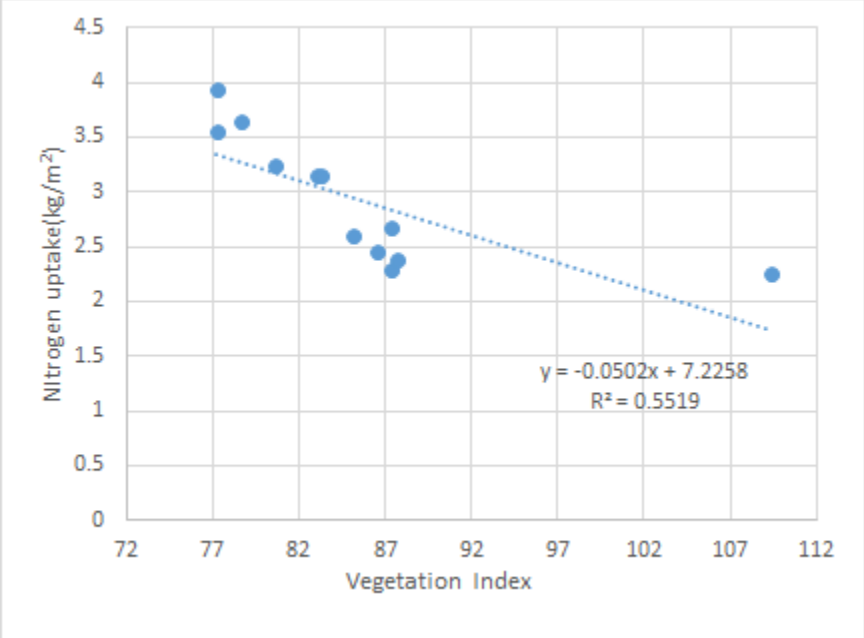

Figure A2. Correlation between N uptake (Aug 4) and yield

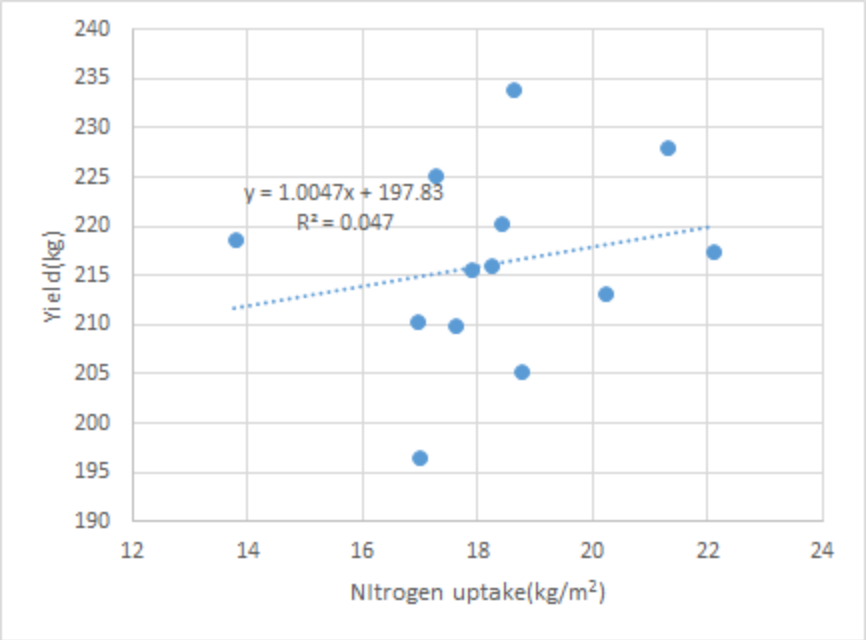

Figure A3. Correlation between N uptake (Sept 4) and yield (stover and grain)

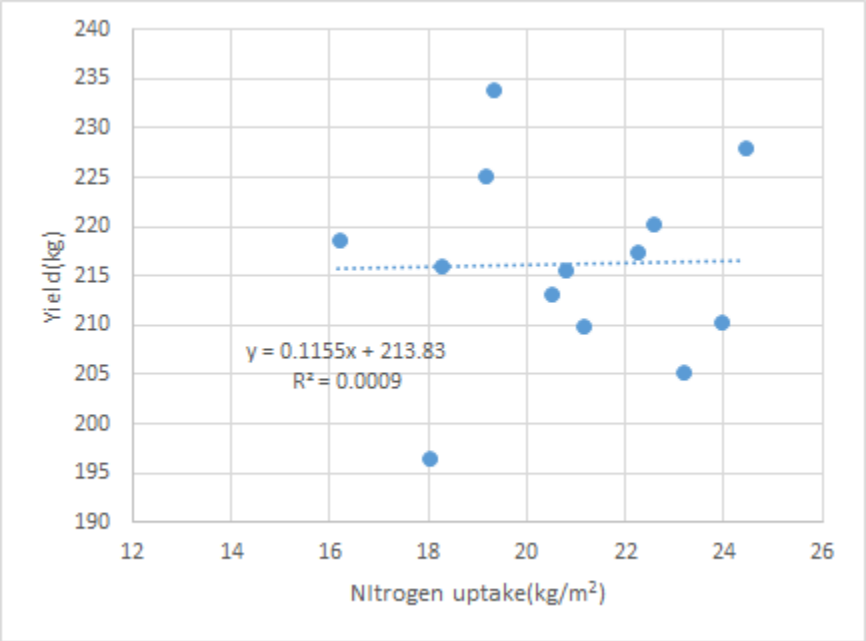

Figure A4. Correlation between N uptake (Oct 8) and yield (stover and grain)

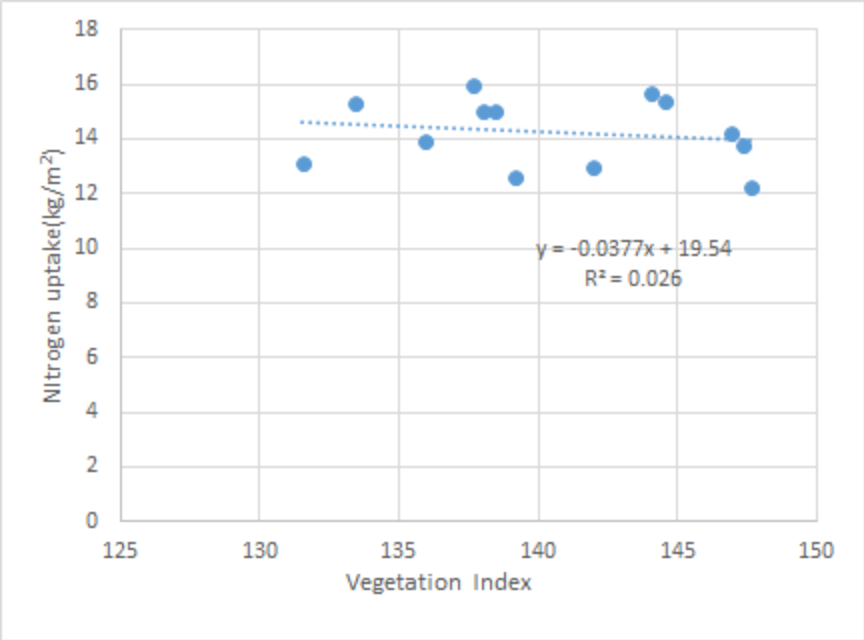

Nitrogen uptake and vegetation indices

Figure A5. N uptake (July 1) and original red reflectance (June 24)

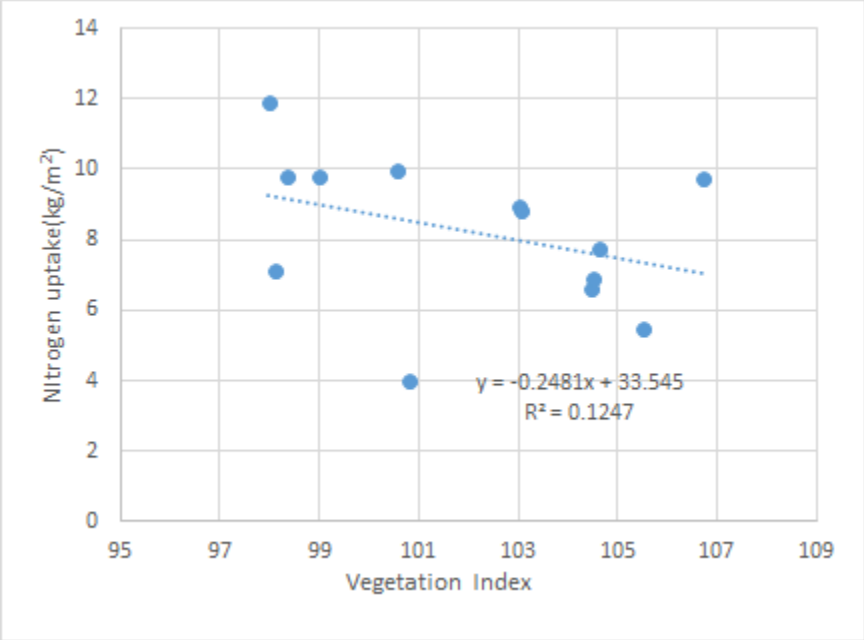

Figure A6. N uptake (Aug 4) and original band index (Aug 4)

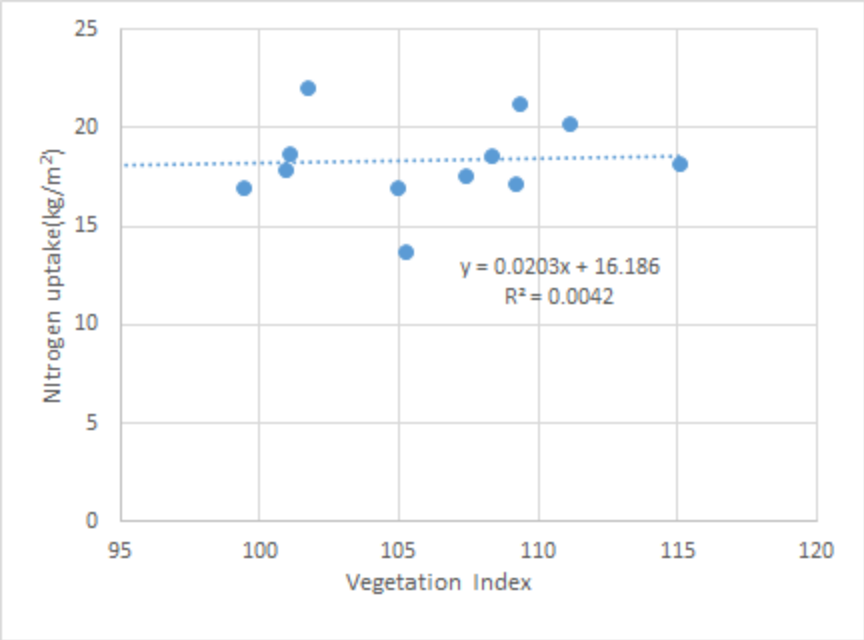

Figure A7. N uptake (Sept 4) and original Red index (Sept 10)

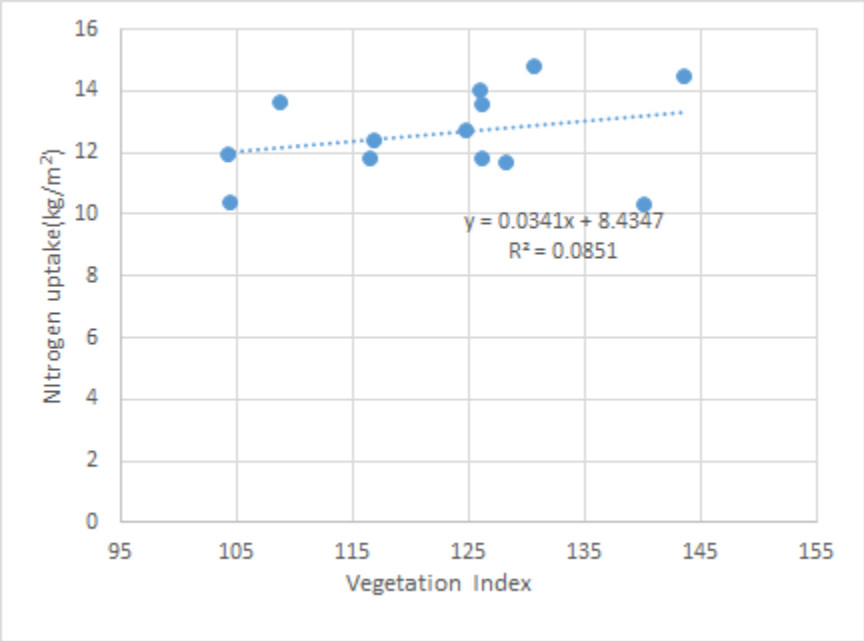

Figure A8. N uptake including stover and grain (Oct 8) and original Red index (Oct 8)

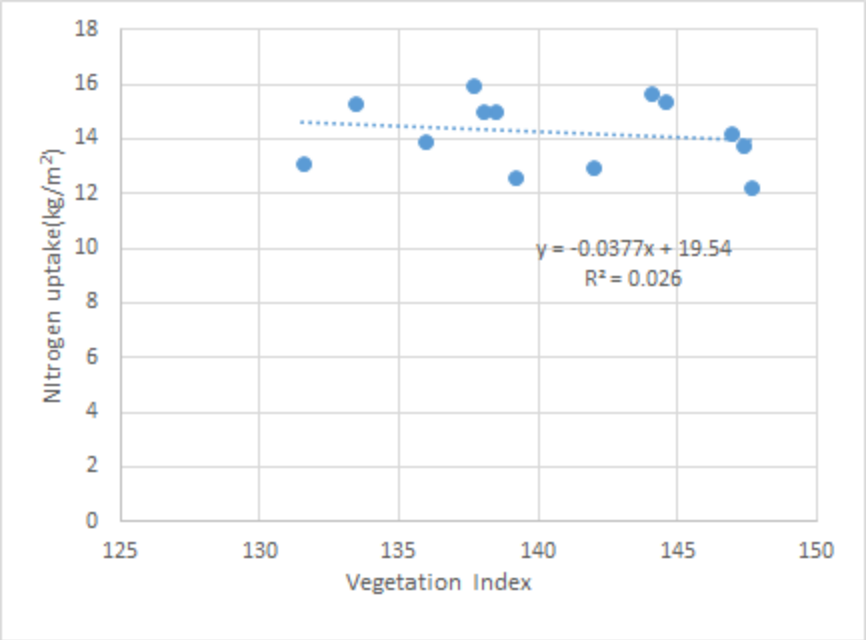

Airscout images-imagery from one date that has been transformed by each of the 11 different wavelength combinations. The image are reported below.

06-09-2015

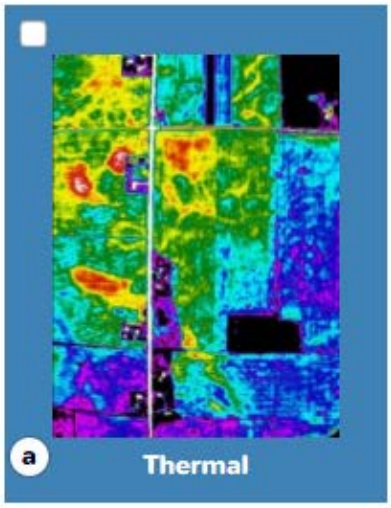

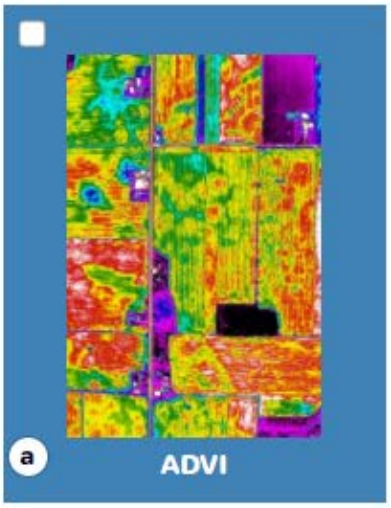

05-14-2015

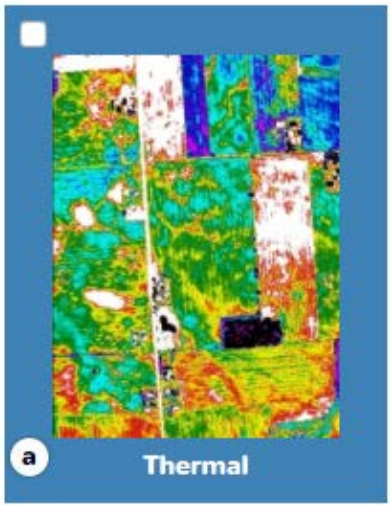

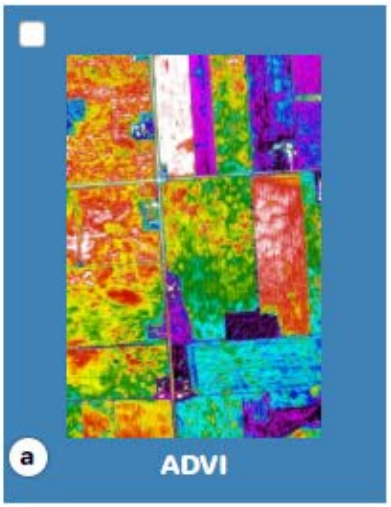

07-08-2015

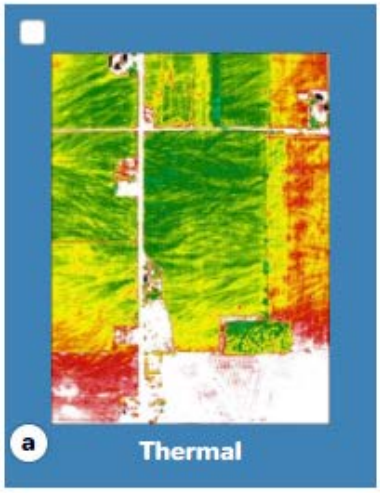

06-24-2015

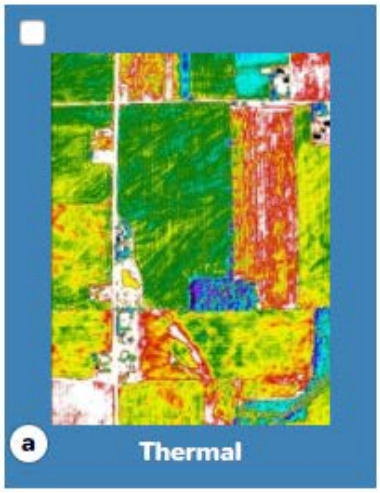

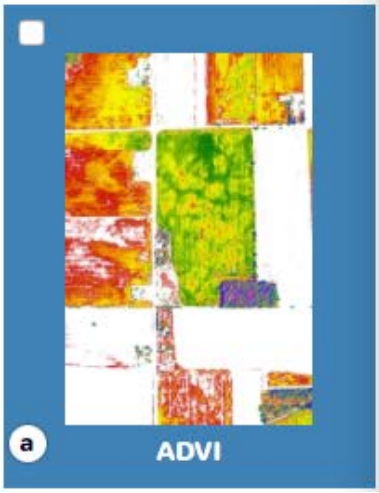

08-04-2015

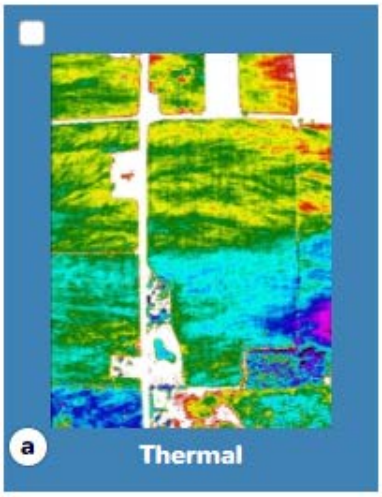

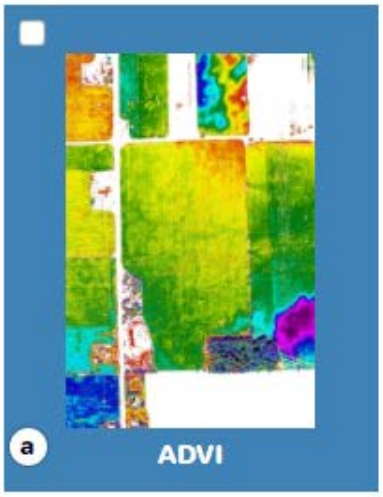

07-27-2015

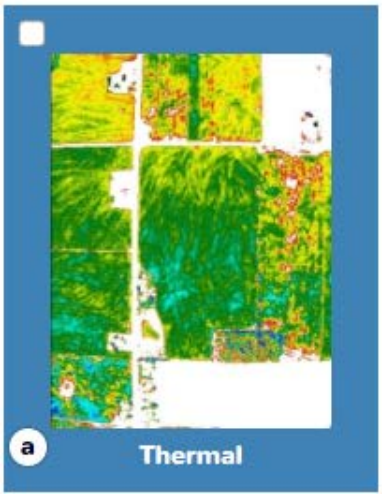

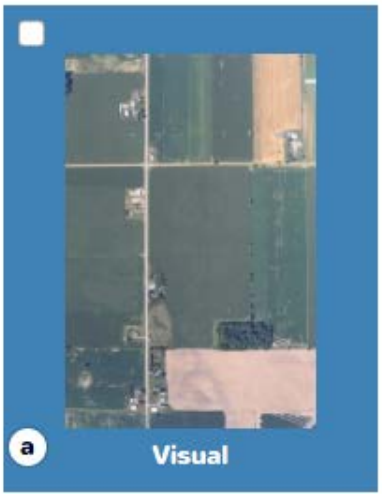

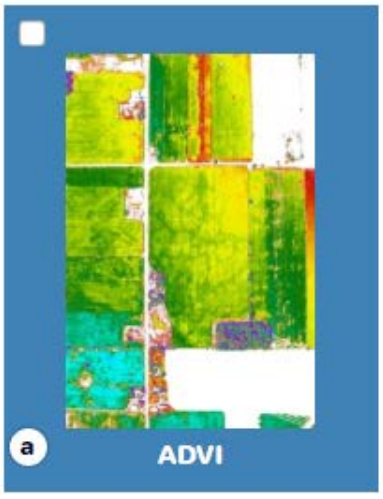

10-08-2015

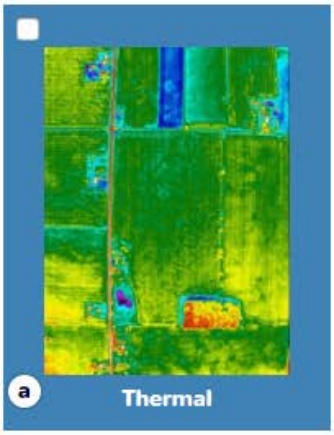

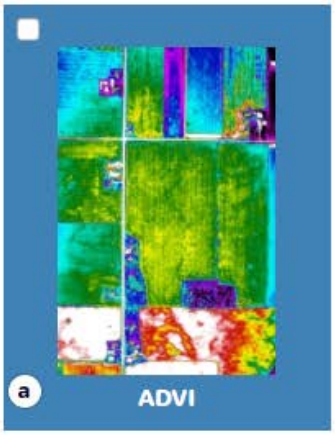

09-21-2015

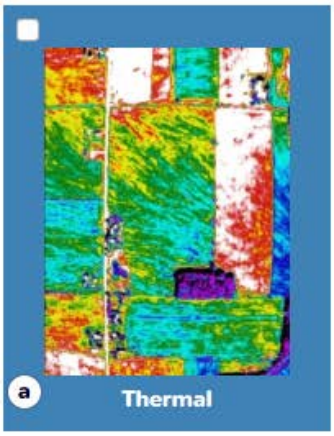

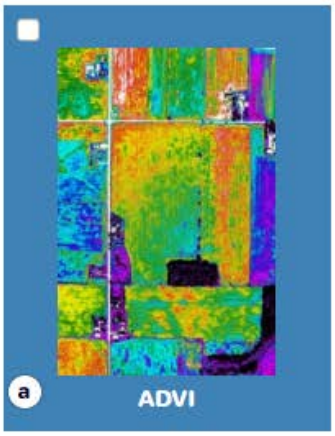
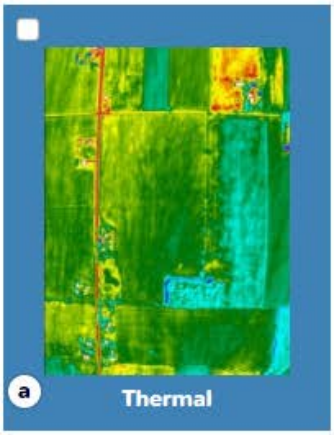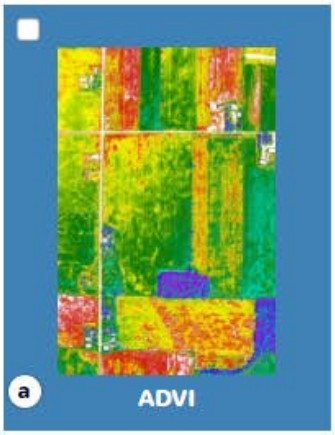
09-10-2015